Seasonality of the ENSO-Related Rainfall Variability in Central Chile and Associated Circulation Anomalies

ALDO MONTECINOS* AND PATRICIO ACEITUNO

Department of Geophysics, Universidad de Chile, Santiago, Chile

(Manuscript received 4 February 2002, in final form 24 July 2002)

ABSTRACT

The seasonality of the ENSO–rainfall relationship in central Chile (30°–41°S) and associated circulation anomalies are studied using correlation and compositing techniques. During El Niño episodes there is a tendency for the occurrence of above-average precipitation between 30° and 35°S in winter [June–July–August (JJA)] and from 35° to 38°S in late spring [October–November (ON)], while rainfall deficit is typically observed from around 38° to 41°S during the following summer [January–February–March (JFM)], when El Niño reaches its maximum development. Opposite rainfall anomalies are characteristic during La Niña events. This study confirms results from previous investigations indicating that enhanced blocking activity over the Amundsen–Bellingshausen Seas area in the southeastern (SE) Pacific during El Niño is a key feature explaining the wet conditions in winter. It is also shown that the same circulation anomaly explains the relatively wet conditions in late spring in the 35°–38°S region during El Niño episodes. Furthermore, the southward displacement from winter to late spring of the area with significant ENSO-related rainfall anomalies seems associated with the seasonal migration of the boundary separating the region under the influence of the subtropical domain from the extratropical domain, where the westerly regime and associated disturbances prevail. Blocking episodes in the SE Pacific during El Niño seem to be part of a wave structure, particularly intense during spring, characterized by a sequence of positive and negative quasi-barotropic height anomalies stretching southeastward from the equator toward the SE Pacific and back to the southwestern Atlantic. On the other hand, anomalously dry conditions in winter and late spring during La Niña are favored by long-lasting and intense ridges at subtropical latitudes over the SE Pacific and South America resulting in a southward migration of the midlatitude storm tracks. In summer, a higher frequency of ridges in the southern tip of the South America during El Niño episodes presumably contributes to reinforcement of the southern edge of the subtropical anticyclone in the SE Pacific, which at this time of the year reaches its southernmost position, resulting in the annual rainfall minimum. On the other hand, an increased frequency of cyclonic circulation anomalies crossing the southern tip of the continent is associated with relatively wet conditions in southern-central Chile, particularly during La Niña events.

1. Introduction

Central Chile (30°–41°S) is located between two regions with contrasting climate. To the north the Atacama desert is one of the driest in the world while the southern portion of the country is one of the wettest regions in the Southern Hemisphere (Miller 1976). Thus, annual rainfall increases from around 100 to 2000 mm from north to south within the region. On the eastern side, the Andes Cordillera acts as an effective barrier isolating the region from the Atlantic influence. Most of rainfall in central Chile is originated by cold fronts associated with migratory low pressure systems embedded in the midlatitude westerlies (Fuenzalida 1982). Additionally, cutoff lows contribute between 5% and 10% to the annual rainfall between 26° and 36°S (Pizarro and Montecinos 2000). The relatively large number of fronts passing through central Chile during austral winter is explained by seasonal changes in the large-scale circulation. Specifically, the subtropical anticyclone in the southeastern (SE) Pacific and the subtropical jet stream are at their northernmost position during this time of the year. Then, the seasonal migration of the boundary between the region under the influence of the Hadley cell and the region under the influence of the westerlies, from around 28° in winter to 35°S in summer, explains the strong rainfall annual cycle characterized by relatively wet winters and dry summers (Fuenzalida 1982). Additional details of the seasonal changes in precipitation in central Chile, in the context of the rainfall annual cycle in subtropical South America are presented in Montecinos et al. (2000a).

The influence of the Southern Oscillation (SO) on

* Current affiliation: Departamento de Oceanografía, Centro de Investigación Oceanográfica (COPAS), Universidad de Concepción, Concepcion, Chile.

Corresponding author address: Aldo Montecinos, Departamento de Oceanografía, COPAS, Cabina 7, Casilla 160-C, Concepcion 3, Chile.
E-mail: amonteci@profc.udec.cl

climate variability in central Chile has been known for a long time. In fact, in the pioneering study of Walker and Bliss (1932), where the SO was originally described, rainfall in central Chile and pressure in Santiago were included in the set of variables defining the SO index for austral winter. Several decades later, many studies have confirmed the existence of a relation between rainfall in central Chile and atmospheric and oceanic anomalies in the tropical Pacific related to the SO (e.g., Rubin 1955; Pittock 1980; Quinn and Neal 1983; Aceituno 1988; Rutllant and Fuenzalida 1991).

Rutllant and Fuenzalida (1991) found that major winter storms in central Chile during El Niño episodes are related to enhanced blocking activity over the Bellingshausen Sea (90°W), linking this phenomenon with observed teleconnection wave trains triggered by anomalous atmospheric heating in the tropical Pacific, as suggested by Karoly (1989). Garreaud (1995) identified two recurrent synoptic schemes during large winter rainstorms in central Chile. One of them is characterized by blocking in the Bellingshausen Sea that contributes to a northward shift of the storm track in the SE Pacific, whereas the other scheme is characterized by blocking over the northeast sector of the Weddell Sea (around 55°S and 40°W) that favors the occurrence of quasi-stationary fronts over central Chile.

Long-term changes in the functioning of the SO (Trenberth and Shea 1987) may explain the significant changes in the strength of the SO–rainfall relationship documented for many regions in South America (Aceituno and Montecinos 1993). Nevertheless, the SO–rainfall relationship in central Chile is quite stable, at least when SST in the central equatorial Pacific is used as an SO index (Aceituno et al. 1989). The latter work also indicates the existence of a significant link between enhanced convection and precipitation in the equatorial region around 180° and anomalous wet conditions in central Chile during austral winter.

Montecinos et al. (2000a) documented the existence of a significant warm-wet–cold-dry relationship between SST in the equatorial Pacific and rainfall in the northern portion of central Chile during winter. They also detected a southward displacement of this ENSO signal from winter to late spring, and opposite ENSO-related rainfall anomalies in the southern portion of central Chile during summer.

In the present study, the atmospheric circulation anomalies associated with the seasonal changes of the relationship between the interannual rainfall variability in central Chile and the ENSO cycle are analyzed. Datasets and their preprocessing are described in section 2. Then, in section 3 the seasonal characteristics of transient and long-persistent 500-hPa height anomalies in the SE Pacific and western South Atlantic are described, as a basis for a study of circulation anomalies during wet and dry conditions in central Chile. Large-scale SST and atmospheric circulation anomalies during anomalously wet and dry seasons are analyzed in section 4, using correlation and compositing techniques. Discussion of the results and main conclusions are presented in sections 5 and 6, respectively.

2. Datasets and preprocessing

a. Rainfall

Monthly data from 49 stations in central Chile, between 30° and 41°S, were considered for the period 1958–99 (Fig. 1). Previous results from Montecinos (1998) and Montecinos et al. (2000a) show that ENSO-related rainfall variability is highly seasonally dependent in central Chile, with most significant relationships occurring in winter [June–July–August (JJA)] from 30° to 35°S (region A), during late spring [October–November (ON)] between 35° and 38°S (region B), and during summer [January–February–March (JFM)] from 38° to 41°S (region C). For each of these regions a seasonal rainfall index was defined as the first principal component (PC1) of standard deviation–normalized rainfall series, considering a total of 24, 16, and 9 stations, for regions A, B, and C, respectively. The percentage of total variance retained by these indices are 82% in region A, 84% in region B, and 78% in region C.

All seasonal rainfall indices exhibit a negative trend, which is consistent with results obtained on an annual basis by Montecinos et al. (2000b). However, a detrend procedure was applied only to the summer rainfall index in region C whose negative trend reaches statistical significance according to a Monte Carlo test (95% of confidence). The relatively large percentage of total variance captured by the PC1 reveals the strong regional coherence in rainfall, that is mostly associated with extratropical cold fronts affecting homogeneously a large portion of the narrow territory between the Pacific coast and the Andes Cordillera (Garreaud 1995). Resulting regional–seasonal rainfall indices are presented in Fig. 1.

b. Gridded fields

Monthly National Centers for Environmental Prediction–National Center for Atmospheric Research (NCEP–NCAR) reanalysis data with a 2.5° × 2.5° latitude–longitude resolution were considered for the period January 1958–December 1998 (Kalnay et al. 1996). Daily 500-hPa geopotential height (H500) data at 1200 UTC from same reanalysis for the period January 1979–December 1999 were also used. According to Kidson and Sinclair (1995) H500 is a good indicator of quasi-barotropic perturbations in the Southern Hemisphere and gives a reasonable position of both the subtropical and polar jets, which have similar strength at this level during austral winter (e.g., Trenberth 1991). As suggested by Renwick and Revell (1999) the mean trend was removed at each grid point in order to avoid spurious trends. Monthly field anomalies were obtained by subtracting the long-term monthly mean at each grid point.

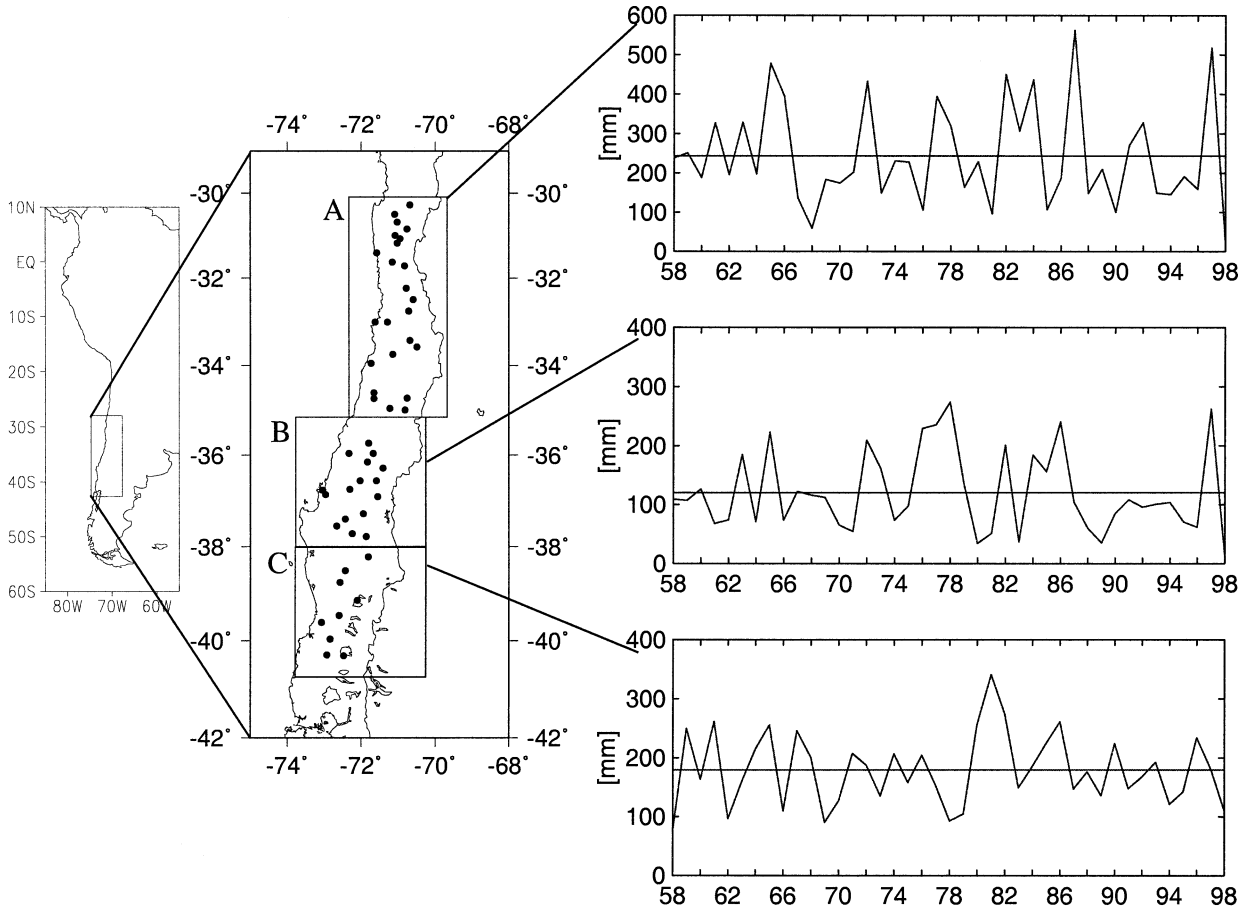

FIG. 1. Seasonal rainfall indices for central Chile (30°–41°S): (top) winter (JJA) in region A (30°–35°S), (middle) late spring (ON) in region B (35°–38°S), and (bottom) summer (JFM) in region C (38°–41°S). Spatial distribution of rainfall stations in each region is indicated.

Two monthly NCEP SST datasets were used: the empirical orthogonal function reconstructed SST analysis of Smith et al. (1996) from January 1958 to December 1981 and the optimal interpolation SST analysis of Reynolds and Smith (1994) from January 1982 to December 1998. Further information about these datasets can be found in Hurrell and Trenberth (1999). Monthly SST anomalies were obtained by subtracting the long-term monthly mean.

3. Analysis of persistent height anomalies

Although the nature of circulation anomalies associated with rainfall variability can be assessed using correlation or compositing techniques on monthly data, it is important to verify the barotropic or baroclinic characteristics of such anomalies at shorter timescales. With that purpose the persistent H500 anomalies were analyzed using the methodology described in Dole (1983).

a. Methodology

At each grid point the daily series of H500 anomalies were calculated as the residual after the annual mean and annual and semiannual harmonics were removed. Previously, the long-term trend of the 21-yr series had also been removed. Height anomalies were normalized by the scale factor sin45°/sin(latitude) following the methodology described by Dole and Gordon (1983). They noted that latitude-normalized anomalies do not mask geographical variations in their intensity and are more amenable to direct physical interpretation in comparison with standard deviation–normalized departures.

The frequency of episodes of normalized positive and negative height anomalies having a magnitude equal or larger than a threshold value during a certain number of days was calculated at each grid point. This method has been used in studies of blocking in the Northern (Dole 1983; Dole and Gordon 1983; Shukla and Mo 1983) and Southern (Trenberth and Mo 1985) Hemispheres. Here, this methodology was used to study the frequency of transient and long-persistent episodes in the region 20°–80°S, 180°–40°W.

Thresholds and durations used to identify episodes are those defined by Trenberth and Mo (1985) and Kiladis and Mo (1998). Thus, for positive (negative) transient events the magnitude of normalized height anomalies had to be equal or larger than 150 gpm during a

period from 1 to 3 days. These circulation anomalies may be interpreted as large-amplitude baroclinic disturbances at the synoptic timescale. In fact, as noted by Kiladis and Mo (1998) and Trenberth and Mo (1985) the seasonal distribution of these transient events resembles the field of 2–8-day bandpass-filtered variance of 500-hPa height shown in Trenberth (1982).

Positive and negative long-persistent events were defined as those when the magnitude of normalized height anomalies were equal to or larger than 100 gpm during a period of at least 7 days. Positive long-persistent events may be regarded as blocking (e.g., Dole and Gordon 1983; Trenberth and Mo 1985), and they usually imply an anomalous breakdown and deviation of the prevailing westerly flow at midlatitudes (Sinclair 1996).

To homogenize the length of periods analyzed during each season, three 90-day intervals were considered: 1 June–29 August (winter), 17 September–15 December (late spring), and 1 January–31 March (summer).

b. Seasonal characteristics

Figure 2 shows the zonal average in the band 140°–40°W of mean frequency of transient and long-persistent events during the period 1979–99. This domain includes the second-most common area in the Southern Hemisphere (SE Pacific) where blocking episodes are observed (Sinclair 1996; Renwick and Revell 1999). As noted by Trenberth and Mo (1985) and Kiladis and Mo (1998), both positive and negative transient events are one order of magnitude more frequent than long-persistent episodes. The fact that the negative transient events are more frequent than the positive ones is also in agreement with results from previous investigations (Trenberth and Mo 1985). A marked difference is found in the latitudinal distribution of positive and negative transient episodes, particularly during late spring and summer (Figs. 2c,e). The relatively large frequency of negative transient events at low latitudes results from the incursions of large-amplitude troughs or cutoff lows from high latitudes into a region where anticyclones are more frequent (Sinclair 1996), while the relatively large number of positive transient anomalies at midlatitudes accounts for intense ridges in the domain of extratropical cyclones.

Figure 2 also shows that positive long-persistent episodes are relatively more frequent than the negative ones. Also, confirming earlier results discussed by Kiladis and Mo (1998) for the SE Pacific region, the frequency of long-persistent events presents a double maximum at about 60° and 35°S in winter (Fig. 2b). Unlike transient events, whose frequency does not change much throughout the year, the frequency of both positive and negative long-persistent episodes exhibits a marked annual cycle with a maximum during winter and a minimum in summer. This feature, also noticed by Sinclair (1996), is consistent with Renwick and Revell (1999) who found that blocking activity in the SE Pacific maximizes in winter and spring.

The seasonal enlargement of the region under the influence of the westerlies during winter is revealed by the wider latitudinal band of the region with high frequency of transient and long-persistent events (Figs. 2a,b), in comparison with late spring and summer. During the latter season both transient and long-persistent events concentrate between 50° and 55°S (Figs. 2e,f).

4. Large-scale circulation anomalies

The atmospheric circulation anomalies associated with seasonal changes in the ENSO–rainfall relationship in central Chile are described using correlation and compositing techniques. The analysis is performed separately for rainfall in region A (30°–35°S) during winter (JJA), in region B (35°–38°S) in late spring (ON), and in region C (38°–41°S) in summer (JFM). Although these months do not fit the usual season definition, their selection was based on when the equatorial Pacific SST–rainfall relationship is strongest in each region, according to results described in Montecinos et al. (2000a). This study also concluded that rainfall in central Chile is not significantly related to ENSO in fall.

a. Winter rainfall in region A (30°–35°S)

Atmospheric and oceanic anomalies associated with interannual rainfall variability in region A are presented in Fig. 3. The scatter diagram in Fig. 3a (correlation of 0.63) shows that rainfall during the period 1958–98 was well above normal in all years when the Niño-3.4 (5°N–5°S, 120°–170°W) SST anomaly was larger than +1.0°C, while it was never in the third (wettest) tercile of the distribution when the SST anomaly was below −0.5°C. Although this situation reveals that winter rainfall in region A is significantly related to extreme SST anomalies in the central equatorial Pacific, it should be noticed that rainfall is widely scattered within the dry, normal, and wet scenarios when near-normal SST conditions prevail in the equatorial Pacific.

The ENSO influence in rainfall variability is further documented in Fig. 3b, depicting the pattern of correlation between the rainfall index and SST in the Pacific and western Atlantic Oceans. Specifically, the correlation pattern in the Pacific domain exhibits the characteristic horseshoe structure of the SST anomaly field during warm episodes, with maximum positive values over the central equatorial Pacific and negative ones to the south of a line stretching southeastward from the equator, at about 160°E. Correlations larger than +0.60 are observed along the equatorial Pacific from 160° to 130°W, approximately.

The SLP–rainfall correlation pattern presented in Fig. 3c also shows the characteristic signature of the SO in the Tropics, particularly the positive correlations over Australia and the Maritime Continent and the negative

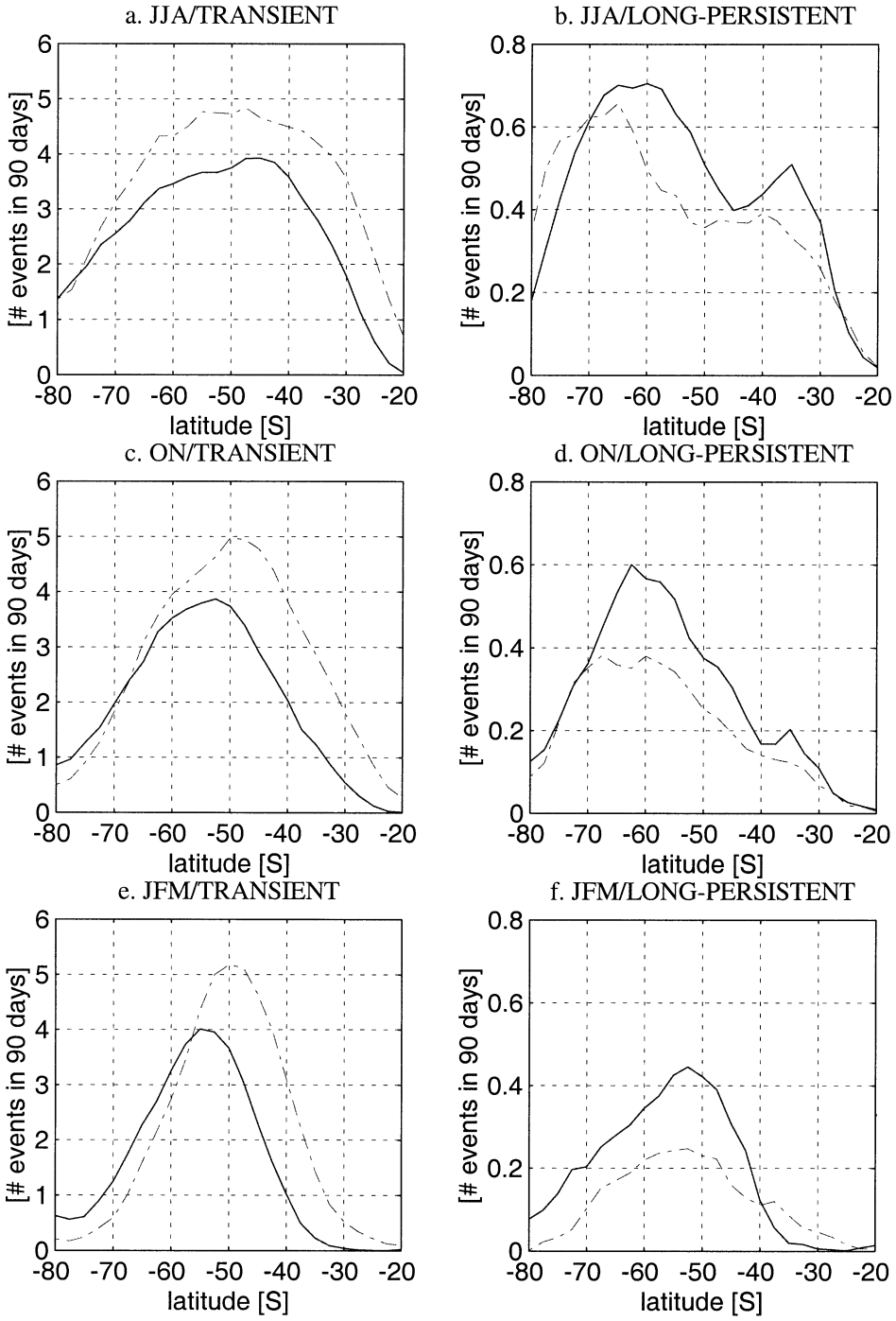

FIG. 2. Meridional profiles of the mean frequency, in the region 140°–40°W, of positive (solid line) and negative (dashed line) (a), (c), (e) transient and (b), (d), (f) long-persistent episodes of 500-hPa height anomalies during (a), (b) winter, (c), (d) late spring, and (e), (f) summer, averaged during 21 yr (1979–99). For the definition of transient and long-persistent events, see the text.

ones over the central and eastern tropical Pacific. This pattern is consistent with a weak (strong) subtropical anticyclone off the coast of northern and central Chile when relatively wet (dry) winter conditions prevail in this region. The pattern of correlation between the rainfall index and 200-hPa height (H200), shown in Fig. 3d is also conditioned by the functioning of ENSO. Thus, the positive correlations over the tropical Pacific indicate a tendency for a relatively warm (cold) troposphere during El Niño (La Niña) episodes. On the other hand,

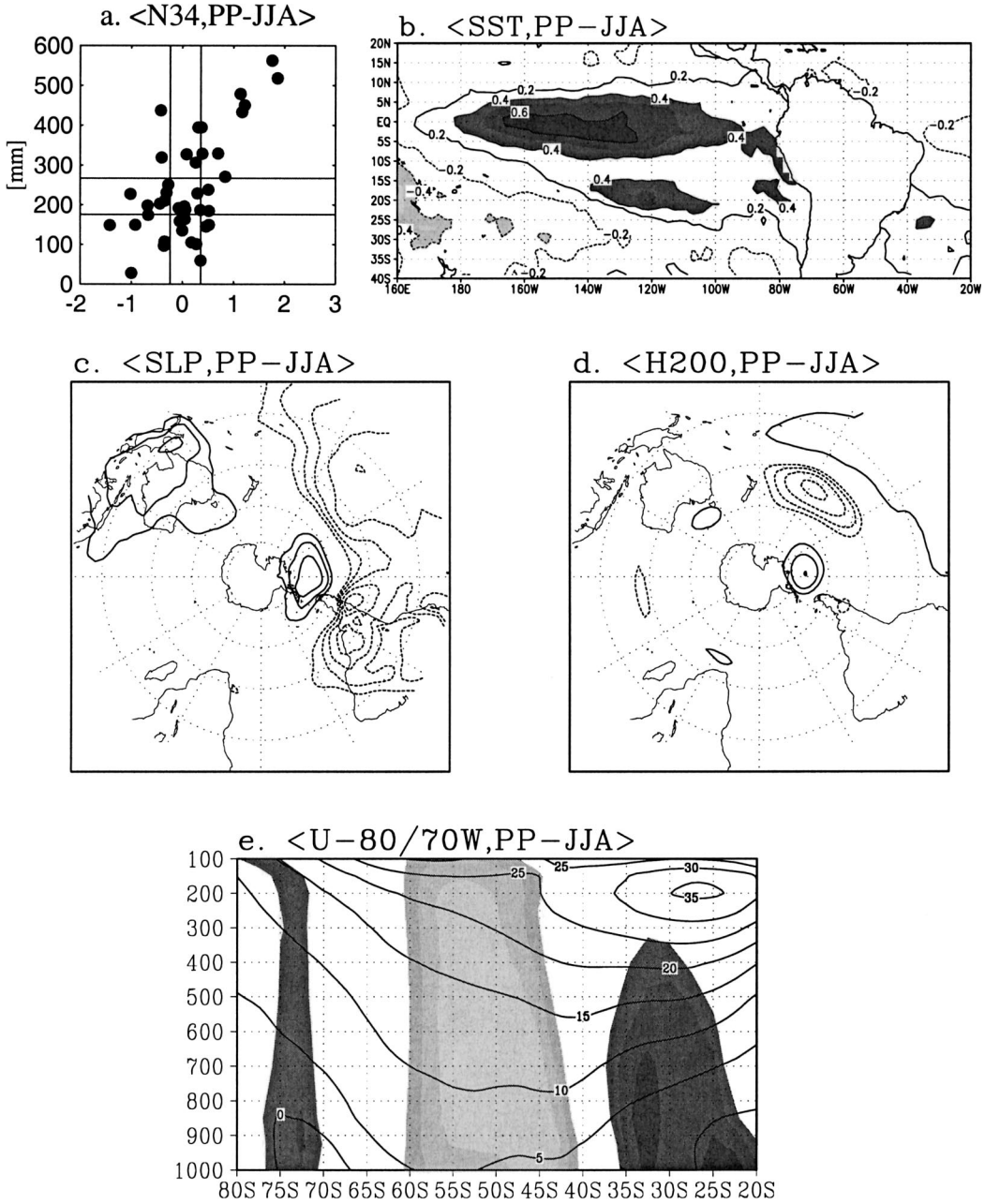

FIG. 3. SST and atmospheric circulation anomalies related to rainfall variability during winter in region A (30°–35°S): (a) Scatter diagram between SST anomalies in the Niño-3.4 region and the rainfall index. Vertical and horizontal lines define limits of terciles. (b) Correlation between the rainfall index and SST anomalies, drawn every 0.2, with magnitudes larger than 0.4 shaded. (c) Correlation between the rainfall index and SLP. Isolines drawn every 0.1 for magnitudes larger than 0.3. (d) As in (c) but for 200-hPa height. (e) Pressure–latitude pattern of correlation between the rainfall index and the zonal wind, averaged between 80° and 70°W. Correlations are shaded every 0.1 for magnitudes larger than 0.3. Continuous (broken) lines in (b), (c), (d), and (e) indicate positive (negative) correlations. Zero isolines are omitted. Solid lines in (e) depict the climatological zonal wind.

negative correlations over central Chile in the SLP and H200 fields, are interpreted as an enhanced (diminished) frequency of low pressure systems and troughs during wet (dry) conditions in this region. This feature is consistent with the increased frequency of cyclones in the subtropical SE Pacific found by Sinclair et al. (1997) during the winter semester (May–October) of El Niño events. The most remarkable feature in the SLP–rainfall and H200–rainfall correlation patterns at midlatitudes (Figs. 3c,d) is the area of significant positive correlations centered in the Amundsen–Bellingshausen Seas (AmBe), around 60°S and 90°W, suggesting an in-

TABLE 1. Wet and dry seasons defined as the third and first tercile of the observed rainfall distribution in the period 1979–99, respectively, for each regional–seasonal rainfall index defined in section 2.

JJA (30°–35°S)		ON (35°–38°S)		JFM (38°–41°S)	
Wet	Dry	Wet	Dry	Wet	Dry
1982	1981	1979	1980	1980	1979
1983	1985	1982	1981	1981	1987
1984	1988	1984	1983	1982	1989
1987	1990	1985	1988	1985	1991
1991	1993	1986	1989	1986	1994
1992	1994	1991	1998	1990	1995
1997	1998	1997	1999	1996	1998

creased frequency of blocking over this area when above-normal winter rainfall occurs in region A.

The pattern of correlation between the rainfall index and the zonal wind component along a tropospheric cross section (1000–100 hPa) off the Chilean coast from 20° to 80°S is presented in Fig. 3e. Zonal winds were averaged in the band 80°–70°W. Results are highly consistent with those presented in Figs. 3c,d. In particular, the dominant negative correlations over the whole troposphere at midlatitudes (40°–60°S) are indicative of relatively weak westerlies associated with blocking over the AmBe region during anomalously wet winters. At the same time, positive correlations in the lower and midtroposphere at the subtropics are indicative of enhanced westerlies at the cyclonic shear side of the climatological subtropical jet when wet winter conditions prevail in region A. At this time of the year the subtropical jet reaches its highest intensity (around 35 m s^{-1}) and northernmost position at about 27°S (Fig. 3e).

Some aspects of the large-scale circulation anomalies suggested by the SLP–rainfall and H200–rainfall correlation patterns (Figs. 3c,d) are further investigated through the frequency pattern of positive and negative long-persistent and transient episodes (calculated as described in section 3) during anomalously wet and dry winters. At each grid point, the frequency of these episodes was added for the wet (rainfall in the third tercile) and dry (rainfall in the first tercile) winters (Table 1). The difference in accumulated frequency (wet minus dry) for each type of episode (long persistent and transient; positive and negative) is mapped in Fig. 4.

The positive values prevailing in the AmBe area in Fig. 4a reveal a larger frequency of blocking episodes over this region when relatively wet conditions prevail in region A, while an increased number of positive long-persistent events in the latitudinal band 40°–45°S during dry conditions would explain the negative values along this band. The pattern of wet–dry difference in the frequency of negative long-persistent episodes in Fig. 4b is broadly opposite to that in Fig. 4a, suggesting that anomalous wet winter conditions are associated with

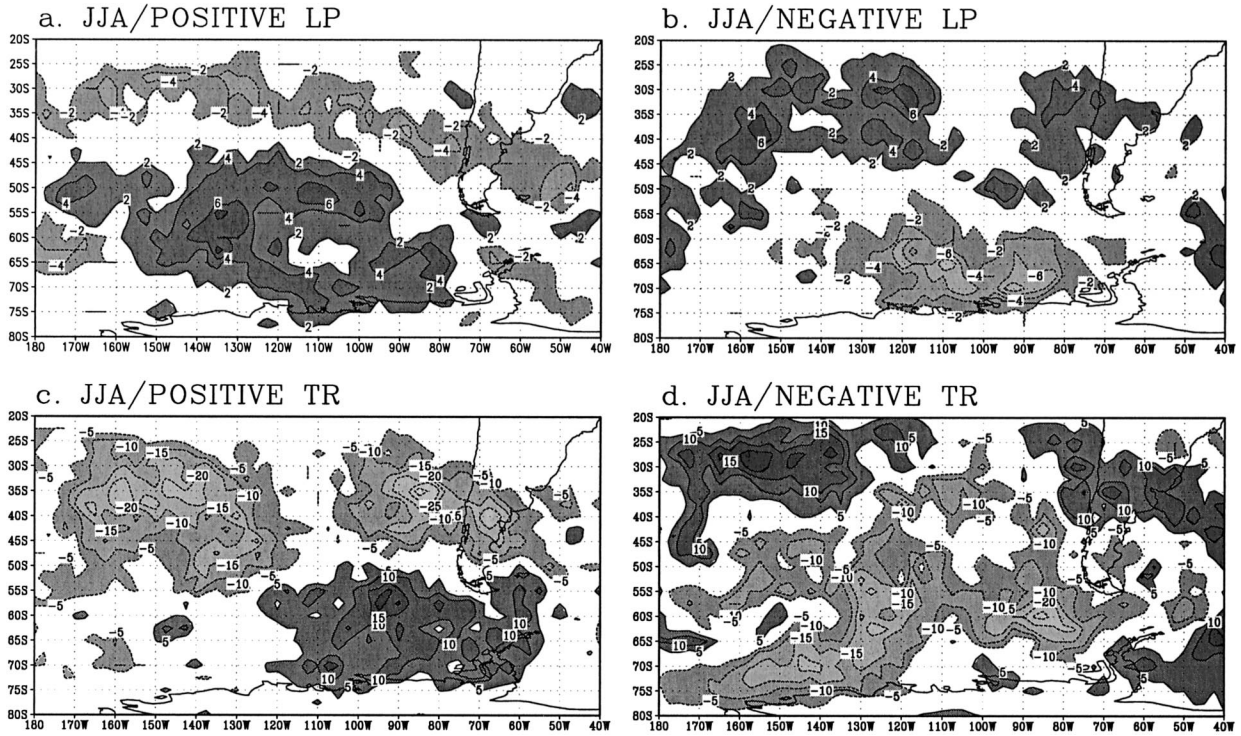

FIG. 4. Patterns of the difference in frequency of transient (TR) and long-persistent (LP) events of 500-hPa height anomalies between anomalously wet and dry winters in region A (30°–35°S): (a) positive and (b) negative LP events; (c) positive and (d) negative TR events. Positive (negative) differences are indicated by continuous (broken) isolines and dark (light) shading. Isolines are drawn every 2 (5) units for LP (TR) episodes, with the zero line omitted.

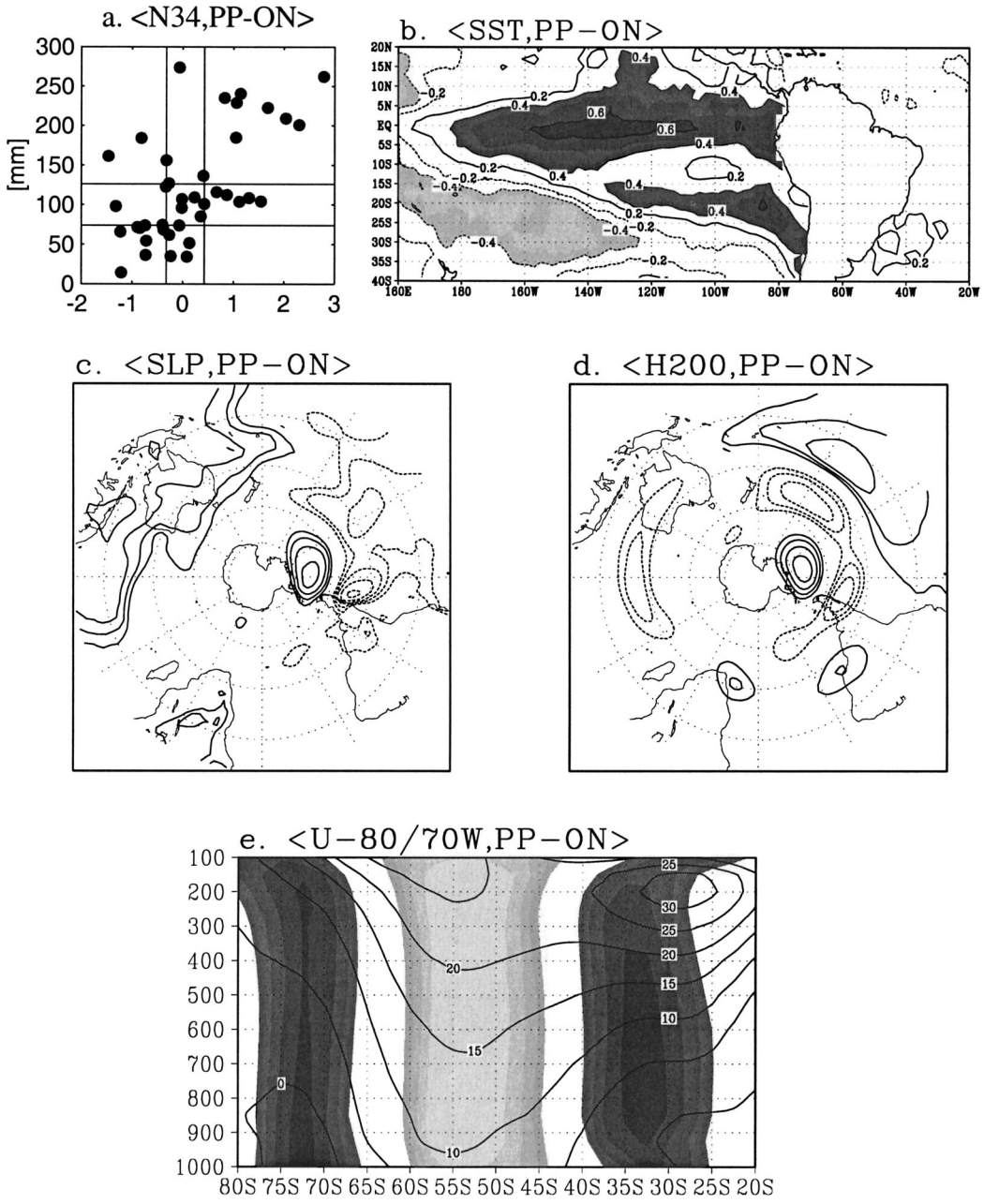

FIG. 5. As in Fig. 3, but for late spring rainfall in region B (35°–38°S).

more frequent negative long-persistent events in the band 30°–35°S, whereas a larger frequency of these episodes in the AmBe region is characteristic for dry winters in region A. Regarding the spatial distribution of transient episodes, Fig. 4c shows that during wet winter conditions positive episodes are more frequent in the region just to the east of where enhanced blocking activity occurs, while during dry conditions they are more frequent along the band 30°–50°S. This pattern is broadly opposite to that observed for negative events. Thus, the predominant positive values in the subtropics depicted in Fig. 4d indicate an increased frequency of transient troughs passing through these latitudes during the wet winter over region A. However, it is worth noting that during dry conditions a higher frequency of negative episodes between 180° and 120°W does not have an opposite counterpart during wet events.

b. Late spring rainfall in region B (35°–38°S)

A similar analysis to that described for winter rainfall in region A, is presented in Figs. 5 and 6 for rainfall in

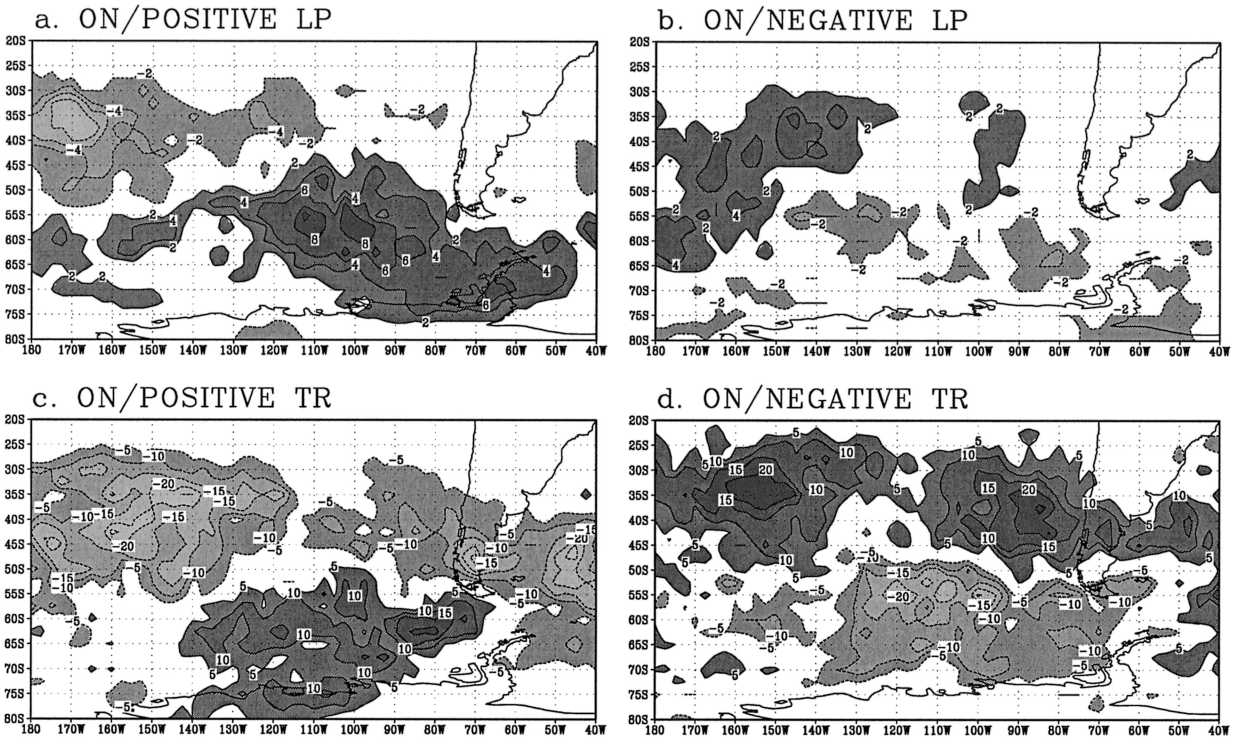

FIG. 6. As in Fig. 4, but for the difference between wet and dry conditions during late spring in region B (35°–38°S).

region B (35°–38°S) during late spring (ON) when the SST–rainfall relationship is strongest (Montecinos et al. 2000a).

The scatter diagram between the rainfall index and SST anomaly in the Niño-3.4 region (correlation of 0.59) indicates a tendency for normal to above-normal late spring rainfall during warm episodes in the equatorial Pacific. The relationship is weaker during cold events, but still in the majority of these cases seasonal rainfall remains in the first tercile of the distribution. Analogous to the situation described for winter rainfall in region A, Fig. 5a shows that rainfall variability is largest when near-normal conditions prevail in the equatorial Pacific. The significant impact of ENSO in late spring rainfall in region B is confirmed by Fig. 5b presenting the correlation pattern between the rainfall index and the SST field. In the tropical Pacific this pattern has the characteristic structure of the SST anomaly field during warm episodes. Maximum correlation values (larger than 0.60) are of the same order of magnitude to those found for winter (Fig. 3b) and concentrates in the equatorial band from 150° to 110°W.

The patterns of correlation between the rainfall index and SLP and H200 are presented in Figs. 5c,d. Similar to those described in the context of rainfall in region A (Figs. 3c,d) they show the signal of the SO in the Tropics, particularly in the contrast between positive SLP–rainfall correlations in the western Pacific, Australia, and Oceania and the negative correlations over the central and eastern tropical Pacific (Fig. 5c). Furthermore, the positive (negative) values in the H200–rainfall correlation pattern (Fig. 5d) over the central equatorial Pacific (subtropical South Pacific) is also an indication of the influence of ENSO in rainfall variability. The region of positive correlations over the AmBe area is the key extratropical feature in the SLP–rainfall and H200–rainfall correlation patterns, suggesting that as in winter, blocking in this region is a recurrent circulation anomaly during the anomalously wet late springs in region B.

The SLP and H200 anomalies inferred from Figs. 5c,d are consistent with the pattern of correlation between the rainfall index and the zonal wind component off the coast of Chile presented in Fig. 5e. Specifically, the negative correlations dominating the entire tropospheric column in the band 45°–60°S indicate a weaker-than-normal westerly flow during blocking in the AmBe region. Furthermore, positive correlations at higher latitudes go along with an increased baroclinicity in the southern flank of the blocking, while the positive correlations in the subtropics are in agreement with the enhanced meridional gradient of geopotential height suggested in Fig. 5d for anomalously wet conditions during late spring. In comparison with the situation described for winter rainfall in region A, the strengthening of the westerly flow during the wet late springs in region B extends to the entire troposphere, including the southern margin of the subtropical jet stream, that is relatively weaker and slightly displaced southward in relation to its winter conditions.

Patterns of the difference in the rate of occurrence of

both positive and negative long-persistent and transient events between wet and dry late springs (Table 1) are presented in Fig. 6. In general terms, results are similar to those described in the context of rainfall extremes in region A during winter (Fig. 4). Thus, the positive values in the AmBe region in Fig. 6a, extended to the Weddell Sea, are indicative of a higher frequency of blocking during anomalously wet conditions. Regarding transient episodes, wet seasons are characterized by a larger frequency of positive events over the AmBe region (Fig. 6c), and an above-average number of negative episodes over central Chile (35°–45°S) and the adjacent subtropical Pacific (Fig. 6d). Furthermore, the negative values along the band 40°–50°S in Fig. 6c are consistent with a higher frequency of positive transient events along this band during dry conditions. Figures 6c and 6d jointly suggest the occurrence of northward (southward) migration of the midlatitude storm tracks over the SE Pacific when anomalously wet (dry) conditions prevail in region B during late spring.

c. Summer rainfall in region C (38°–41°S)

Contrary to what is observed in regions A and B during winter and late spring, respectively, there is a significant tendency for the occurrence of relatively dry (wet) conditions along the southern part of central Chile (38°–41°S) during summers coinciding with El Niño (La Niña) episodes. This tendency is revealed in the scatter diagram between the summer rainfall index and simultaneous Niño-3.4 SST index (correlation of −0.44; Fig. 7a). Rainfall remains in the first tercile of the distribution in most summers with SST anomalies above +1.0°C, while normal to above-normal precipitation is typically observed when relatively cold conditions prevail in the central equatorial Pacific. This ENSO signal on rainfall variability is revealed in the SST–rainfall correlation pattern presented in Fig. 7b, whose structure is quite similar to that of the SST anomaly field during cold episodes in the equatorial Pacific. However, the maximum SST–rainfall correlations in the equatorial Pacific are weaker in this case, as compared with those in winter (Fig. 3b) and late spring (Fig. 5b).

Correlation patterns between the rainfall index and SLP (Fig. 7c) and H200 (Fig. 7d) are considerably weaker than the analogous ones for winter and late spring rainfall in regions A and B (Figs. 3c,d and 5c,d). Thus, the weak negative H200–rainfall correlations in the Tropics indicate a tendency for above-average geopotential height when conditions are dry, which is consistent with the H200 anomalies during warm episodes in the tropical Pacific. The positive correlations in the subtropical South Pacific are also coherent with the ENSO signal detected in the rainfall index, in the sense that negative height anomalies prevail in that region during warm episodes in the equatorial Pacific. At higher latitudes, the most significant feature is the quasi-barotropic circulation anomaly suggested by the negative SLP–rainfall and H200–rainfall correlations around the southern tip of the South America.

The correlation pattern between the rainfall index and the zonal wind component averaged in the band 80°–70°W (Fig. 7e) is consistent with results in Figs. 7c,d. In particular, the negative values around 50°S in the southern tip of the continent in the SLP–rainfall and H200–rainfall correlation pattern are coherent with a weakened (enhanced) baroclinicity to the south (to the north) during wet summers. This is consistent with the negative correlations south of 55°S and positive correlations in the band 35°–50°S in Fig. 7e, indicating that wetter (drier) than normal conditions are associated with stronger (weaker) westerlies over region C. During this season, a single subpolar jet located at about 50°S is the dominant feature in the cross section of zonal wind, although a weak subtropical jet appears at 35°S.

The difference in the frequency of long-persistent events, both for positive and negative ones, between wet and dry summer conditions (Table 1), does not exhibit a coherent pattern near the southern tip of South America (Figs. 8a,b). A coherent spatial distribution of larger frequency of positive long-persistent episodes is present around 45°S and 110°W in association with wet conditions in region C. Regarding transient events, Fig. 8c (Fig. 8d) suggests that dry (wet) summers are associated with a relatively larger frequency of positive (negative) events over the southern tip of the continent. Similar to long-persistent episodes an increased number of positive transient events appear around 45°S–110°W during wet summers. During dry summers the latter feature has a counterpart in the enhanced number of negative transient events in the same region.

Finally, it is interesting to mention that the spatial coincidence between enhanced frequency of both long-persistent and transient events in several regions could be indicative of the interaction between the barotropic and baroclinic components of the extratropical circulation during the life cycle of blocking episodes, as described by Trenberth and Mo (1985) and Marques and Rao (1999) for specific events in the South Pacific Ocean.

5. Discussion

The ENSO impact on interannual rainfall variability in central Chile is best defined in region A during winter and region B in late spring. Above-normal rainfall is associated with El Niño events (or the negative phase of the SO) and associated large-scale circulation anomalies: a relatively weak subtropical anticyclone in the southeastern Pacific; positive SST anomalies in the central equatorial Pacific; a warmer-than-average troposphere over the tropical Pacific; and strengthened westerly flow in the subtropics off the coast of central Chile. Opposite SST and atmospheric anomalies typically occur when relatively dry conditions prevail in the aforementioned regions and seasons. During summer the in-

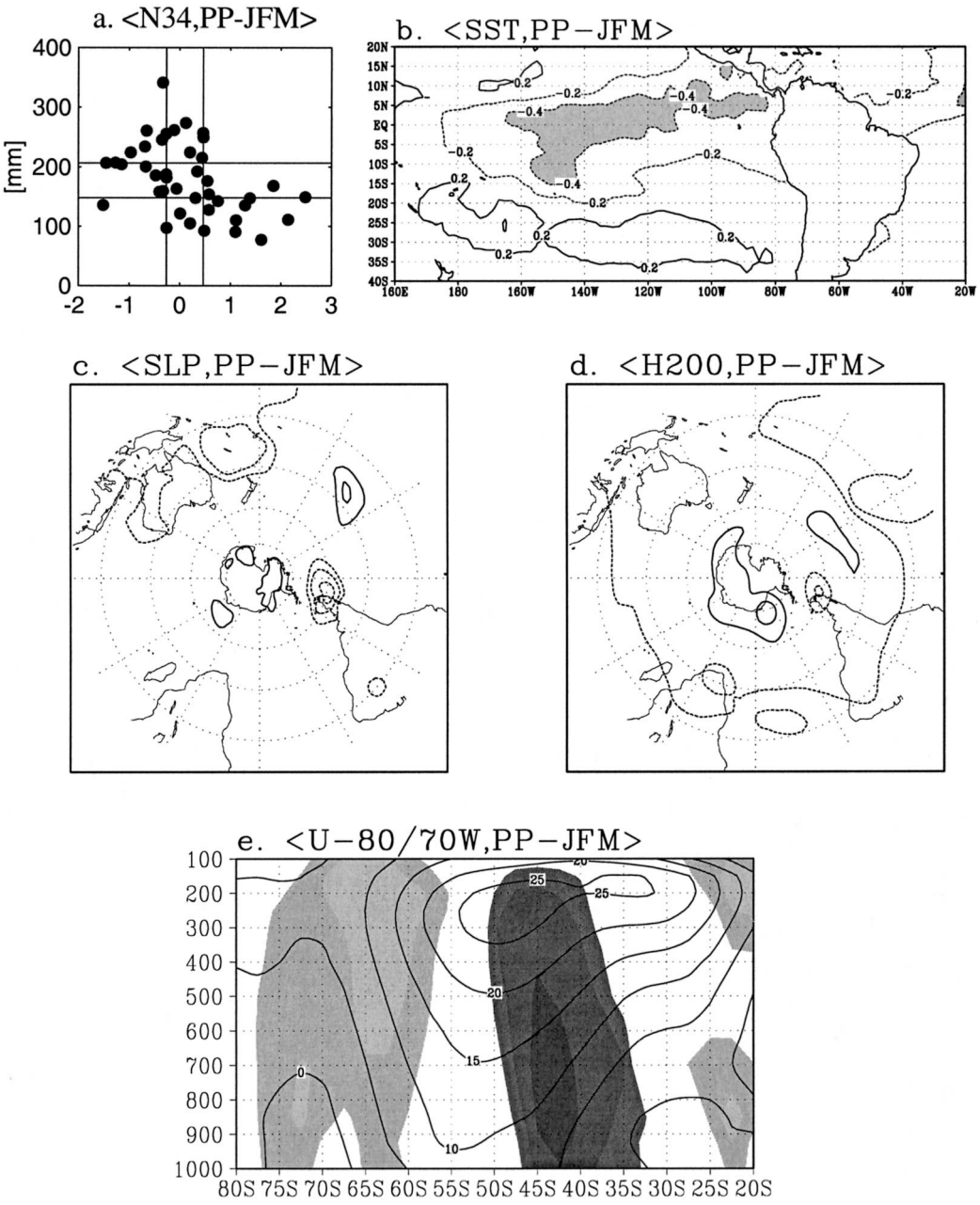

FIG. 7. As in Fig. 3, but for summer rainfall in region C (38°–41°S).

fluence of ENSO on rainfall is considerably weaker and reaches significance only in the southern portion of central Chile (region C) where contrary to what has been described for winter and late spring, rainfall is negatively correlated with SST in the equatorial central Pacific. This kind of ENSO–rainfall relationship is quite uncommon in subtropical South America throughout the year (Montecinos et al. 2000a).

One of the key extratropical circulation anomalies revealed in the correlation and compositing analysis (Figs. 3–6) is blocking over the AmBe area during wet conditions in winter and late spring. A relevant question raised by these results is whether these blocking episodes and the associated circulation anomalies are characteristic features during all wet winters and late springs in central Chile, or if they manifest mostly during El Niño events. To elucidate this matter, SST conditions in the equatorial Pacific were classified as cold, neutral, or warm, depending on if the Niño-3.4 SST index was in the first, second, or third tercile of its empirical distribution during the period 1958–98. Then, the H200 anomaly field was composited (averaged) separately for wet winters when warm and neutral conditions prevailed in the Niño-3.4 region (nine and three cases, respec-

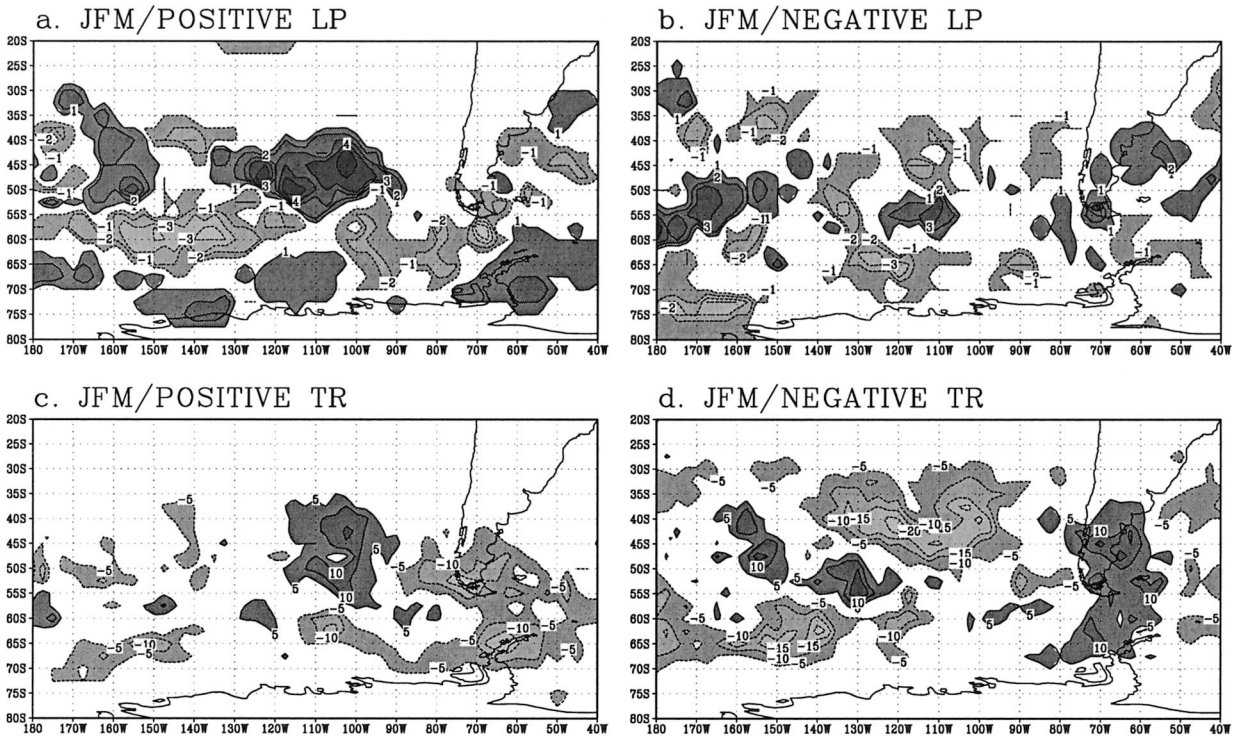

FIG. 8. As in Fig. 4, but for the difference between wet and dry conditions during summer in region C (35°–38°S). Note that isolines for LP events are drawn every 1 unit.

tively). The same composite procedure was repeated for late spring rainfall in region B (nine and four cases, respectively).

Figures 9a,c show that blocking in the AmBe region is a well-defined feature during anomalously wet winters and late springs coinciding with El Niño events, while this circulation anomaly does not appear during wet seasons characterized by neutral SST conditions (Figs. 9b,d). Although the sample size for the latter conditions is small for assessing statistical significance, it is worth noticing that the blocking was absent in each wet winter and late spring season characterized by neutral SST conditions. Furthermore, blocking in the AmBe area during wet winters (Fig. 9a) and especially during late springs (Fig. 9c) seems to be part of a planetary wave structure characterized by a sequence of positive and negative H200 anomalies stretching southeastward from the equator toward the southeastern Pacific and back to the southwestern Atlantic. These results are consistent with those of Rutllant and Fuenzalida (1991) and Garreaud (1995) indicating that blocking in the AmBe region is a conspicuous feature during anomalously wet winters in central Chile that coincide with El Niño events. They also suggest that blocking is part of a characteristic winter teleconnection pattern described by Karoly (1989) for the Southern Hemisphere during El Niño events. This wave train has been identified as the *Pacific–South American* (PSA) teleconnection pattern by Mo and Ghil (1987) or the South Pacific wave train pattern by Kidson (1999).

The fact that blocking in the AmBe region and the associated wave train pattern are stronger in springtime (Fig. 9c) agrees with results from recent studies of blocking over the SE Pacific (Renwick and Revell 1999; Marques and Rao 2000; Rao et al. 2000). According to Renwick and Revell (2000) the observed springtime peak in Southern Hemisphere Rossby wave activity may be a compromise between the strength of the tropical diabatic heating anomaly (maximized in the summer of warm ENSO events) and the strength of the vorticity gradient of the background flow (maximized in winter due to subtropical jet stream reaching its maximum intensity during this season).

Furthermore, Figs. 9a,c indicate that enhanced blocking activity during wet conditions in winter and late spring occurs at a longitude (about 90°W) eastward from the climatological position of the secondary maximum of blocking activity in the SE Pacific (e.g., Sinclair 1996). Renwick and Revell (1999) suggest that this location, where the spectral energy of an SE Pacific blocking index peaks on an interannual timescale (2–4 yr), may reflect the mean pattern of variation over a large ensemble of high-frequency Rossby wave passages, forced by continually varying tropical convection on intraseasonal timescales. Hence, we speculate that blocking at 90°W could be part of the eastward prop-

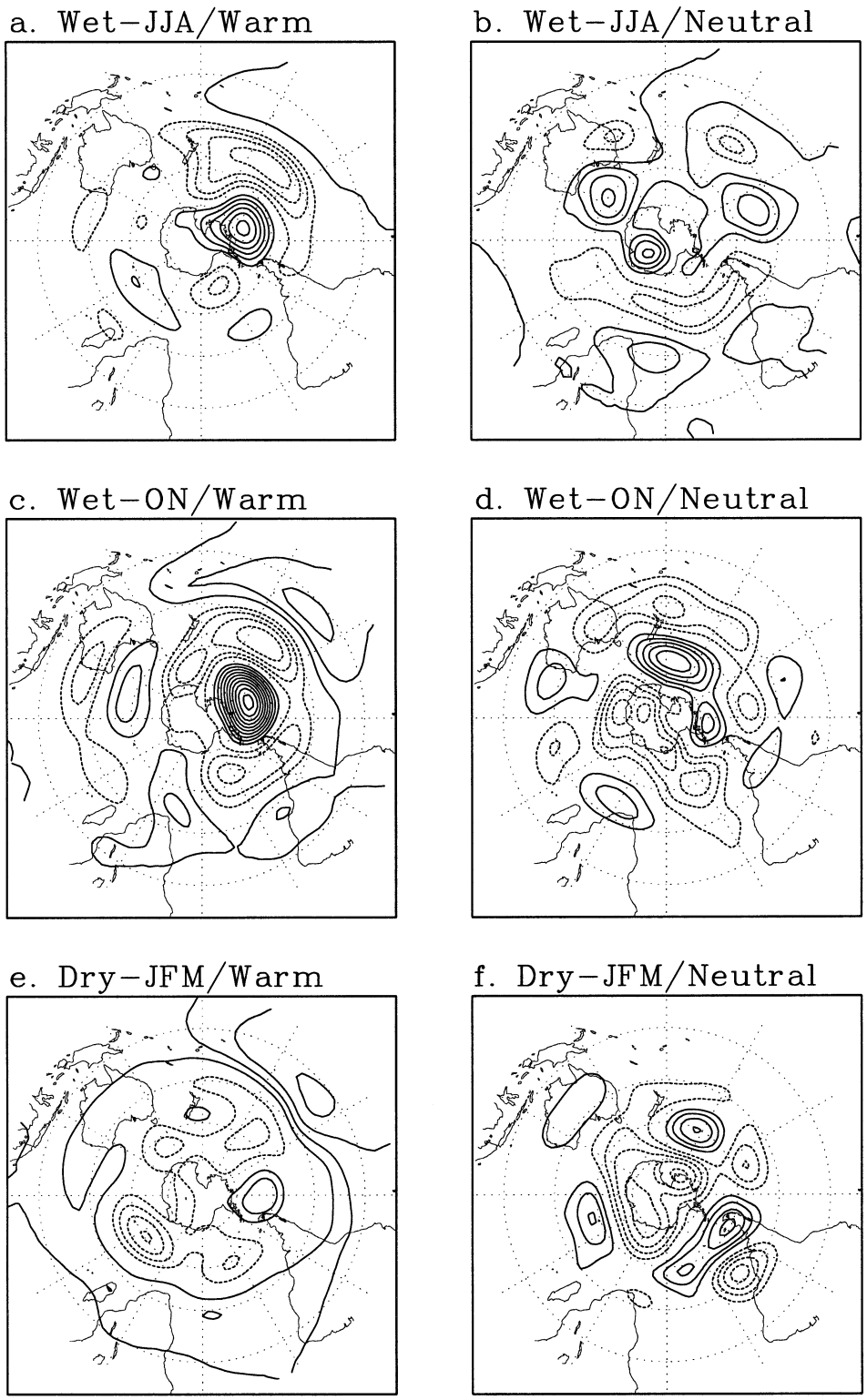

FIG. 9. Composite maps of 200-hPa height anomalies for anomalously wet and dry seasons in central Chile, when (a), (c), (e) warm and (b), (d), (f) neutral conditions prevail in the central equatorial Pacific. Panels (a) and (b) show wet conditions during winter in region A (30°–35°S); (c) and (d) show wet conditions during late spring in region B (35°–38°S); (e) and (f) show dry conditions during summer in region C (38°–41°S). Continuous (broken) lines indicate positive (negative) anomalies. Isolines are drawn every 10 gpm, with zero line omitted.

agation of the same Rossby waves producing blocking in the SE Pacific, especially during warm ENSO events. In fact, blocking over the AmBe region during wet conditions in central Chile may correspond to the breakdown phase of eastward-progressing blocking episodes in the SE Pacific (see Fig. 6 in Renwick and Revell 1999). Additionally, correlation patterns described in Figs. 3c,d and 5c,d show similarities with those between the Niño-3.4 SST index and the SLP and H200 anomaly fields during winter and late spring (not shown). In particular, the region with positive values over the SE Pacific in the SLP–Niño-3.4 and H200–Niño-3.4 correlation patterns is slightly displaced to the west of the AmBe region. Compositing analysis of extratropical height anomalies during individual rainfall events should be studied to clarify this hypothesis.

In the context of an investigation about large-scale circulation features associated with large winter rainstorms in central Chile, Garreaud (1995) identified two major synoptic schemes. The most frequent one includes blocking in the AmBe region. However, the second one is characterized by blocking in the northeast of the Weddell Sea (around 55°S and 40°W), that favors the occurrence of quasi-stationary fronts over central Chile. According to our study this synoptic scheme is not related to ENSO and further analysis is needed to assess its impact on the interannual rainfall variability in central Chile.

Considering that the ENSO–rainfall relationship in region C during summer is opposite to that described for winter and late spring, the H200 anomaly field corresponding to anomalously dry conditions in this region during this season were compared for warm and neutral years in the central equatorial Pacific (nine and three cases, respectively; Figs. 9e,f).

The composite H200 anomaly field for dry seasons coinciding with El Niño events (Fig. 9e) shows the typical pattern of positive anomalies along the Tropics and mostly negative departures in the subtropics, which is documented in other studies for El Niño episodes (Karoly 1989; Kiladis and Mo 1998). A significant feature at midlatitudes is the area of positive anomalies near the southern tip of South America, which is consistent with the negative SLP–rainfall and H200–rainfall correlations shown in Figs. 7c,d. Nevertheless, other studies have indicated a zonally symmetric structure during El Niño characterized by positive height anomalies over the Antarctic and surrounding oceans and negative departures between 35° and 50°S (Mo and White 1985; Karoly 1989; Kiladis and Mo 1998). In fact, when H500 anomaly fields are averaged for all El Niño years in the period 1958–98 (not shown), positive deviations appear over the Antarctic, although they are considerably weaker in relation to those presented in Fig. 8.4c in Kiladis and Mo (1998). The detrend procedure applied in our study could be a factor in the lack of agreement.

The positive height anomalies near the southern tip of South America (Fig. 9e) seem to be originated by a larger frequency of transient and large-amplitude ridges during dry summer conditions in region C (Fig. 8c). On the other hand, Fig. 8d is indicative of a larger frequency of low pressure systems passing over the southern tip of the continent during wet summers. Positive height anomalies are also observed over the southern extreme of South America during dry summers coinciding with neutral SST conditions in the equatorial Pacific (Fig. 9f), as part of a zonal structure of wavenumber 3 at midlatitudes, which is not connected with the Tropics.

The positive (negative) SLP and height anomalies in the southern extreme of South America during dry summers, which seems weakly modulated by ENSO, may contribute to an intensification (weakening) of the southern border of the subtropical anticyclone, which reaches its southernmost position in its annual cycle during summer. This would be a factor contributing to a reduction (an enhancement) of the frequency of extratropical fronts arriving in region C during summer.

In contrast to the situation discussed for winter and late spring, wet and dry summer conditions are not associated with significant changes in the frequency of positive long-persistent events, as revealed by the results in Figs. 8a,b, and the substantially more poleward tilt with height in the vertical structure of the zonal wind correlation in Fig. 7e, when compared with the same structure in winter and late spring (Figs. 3e and 5e). This is consistent with evidence of a substantial weakening of wavelike teleconnection patterns over the South Pacific during summers of El Niño events (e.g., Cook 1998; Rao et al. 2000), although the single subpolar jet that dominates the Southern Hemisphere during this time of the year may potentially serve as a waveguide for planetary wave propagation (Berbery et al. 1992).

Circulation anomalies favoring the occurrence of anomalously dry and wet conditions in central Chile could be modulated by other factors apart from ENSO. For instance, the recently identified Antarctic Circumpolar Wave (White and Peterson 1996), which has been linked to rainfall variability in New Zealand (White and Cherry 1999) and Australia (White 2000), could also play a role on the rainfall variability in central Chile.

6. Concluding remarks

The atmospheric circulation anomalies associated with the seasonal change of the relation between rainfall in central Chile (30°–41°S) and the ENSO cycle have been analyzed. The El Niño (La Niña) associates with above (below) average rainfall in central Chile during winter (30°–35°S) and late spring (35°–38°S), and with dry (wet) conditions in southern-central Chile (38°–41°S) in summer. Thus, regional and large-scale circulation features during extreme rainfall conditions in central Chile share significant similarities with those during the extreme ENSO phases.

In winter, when the boundary between tropical and extratropical air masses is at its northernmost position

in the annual cycle, enhanced blocking activity over the Amundsen–Bellingshausen Seas area and the increased tropical–extratropical temperature gradient during El Niño episodes contribute to a northward migration of the storm track in the SE Pacific and wetter-than-average conditions in central Chile (30°–35°S). These mechanisms remain valid during late spring, although the seasonal southward displacement of the polar border of the subtropical anticyclone could explain that the strongest ENSO signal moves toward 35°–38°S. Blocking at midlatitudes associated with ENSO–rainfall variability in central Chile seems to be part of a planetary wave train originated in the Tropics during warm episodes, which is particularly intense during spring. On the other hand, dry conditions in central Chile in winter and late spring are favored by long-lasting and intense ridges in subtropical latitudes and a southward migration of the midlatitude storm track in the SE Pacific, which are relatively more frequent during La Niña events.

In austral summer the influence of ENSO on the Southern Hemisphere is relatively weak. Still, a significant inverse SST–rainfall relationship is observed in the southern portion of central Chile (38°–41°S). The tendency for the occurrence of relatively dry conditions during El Niño episodes is associated with a larger frequency of anticyclonic circulation anomalies near the southern tip of South America. This may contribute to the strengthening of the southern border of the subtropical anticyclone, which is located at its southernmost position during this time of the year. On the other hand, the relatively wet conditions during La Niña are associated with enhanced frequency of low pressure systems crossing over the southern extreme of the continent.

Acknowledgments. We wish to thank J. Rutllant, G. Kiladis, and an anonymous reviewer for their helpful comments to the original manuscript. This work was supported by Conicyt-Chile through Grant Fondecyt 1010570. NCEP–NCAR reanalysis data were provided by the Climate Diagnostic Center (NOAA). Rainfall data was supplied by the National Weather Service (DMC) and the Bureau of Water Management (DGAMOP). Most figures were created using the Grid Analysis and Display System (GrADS).

REFERENCES

Aceituno, P., 1988: On the functioning of the Southern Oscillation in the South American sector. Part I: Surface climate. *Mon. Wea. Rev.,* **116,** 505–524.

——, and A. Montecinos, 1993: Stability analysis of the relation between the Southern Oscillation and rainfall in South America (in Spanish). *Bull. Inst. Fr. Etudes Andines,* **22,** 53–61.

——, A. del Río, and J. Rutllant, 1989: Rainfall anomalies in the subtropical west coast of South America. Part I: Relationship with SST and convective activity over the central Pacific. Preprints, *Third Int. Conf. on Southern Hemisphere Meteorology and Oceanography,* Buenos Aires, Argentina, Amer. Meteor. Soc., 162–166.

Berbery, E. H., J. Nogués-Paegle, and J. D. Horel, 1992: Wavelike Southern Hemisphere extratropical teleconnections. *J. Atmos. Sci.,* **49,** 155–177.

Cook, K., 1998: On the response of the Southern Hemisphere to ENSO. Preprints, *23th Annual Climate Diagnostic and Prediction Workshop,* Miami, FL, Amer. Meteor. Soc., 323–326.

Dole, R. M., 1983: Persistent anomalies of the extratropical Northern Hemisphere wintertime circulation. *Large-Scale Dynamical Processes in the Atmosphere,* B. J. Hoskins and R. P. Pearce, Eds., Academic Press, 95–110.

——, and N. D. Gordon, 1983: Persistent anomalies of the extratropical Northern Hemisphere wintertime circulation: Geographical distribution and regional persistence characteristics. *Mon. Wea. Rev.,* **111,** 1567–1586.

Fuenzalida, H., 1982: A country of extreme climate. *Chile: Essence and Evolution* (in Spanish), H. García, Ed., Instituto de Estudios Regionales de la Universidad de Chile, 27–35.

Garreaud, R. D., 1995: Regional atmospheric configurations during major storms in central Chile (in Spanish). *Meteorologica,* **19,** 73–81.

Hurrell, J. W., and K. E. Trenberth, 1999: Global sea surface temperature analyses: Multiple problems and their implications for climate analysis, modeling, and reanalysis. *Bull. Amer. Meteor. Soc.,* **80,** 2661–2678.

Kalnay, E., and Coauthors, 1996: The NCEP/NCAR 40-Year Reanalysis Project. *Bull. Amer. Meteor. Soc.,* **77,** 437–471.

Karoly, D. J., 1989: Southern Hemisphere circulation features associated with El Niño–Southern Oscillation events. *J. Climate,* **2,** 1239–1252.

Kidson, J. W., 1999: Principal modes of Southern Hemisphere low-frequency variability obtained from NCEP–NCAR reanalyses. *J. Climate,* **12,** 2806–2828.

——, and M. R. Sinclair, 1995: The influence of persistent anomalies on Southern Hemisphere storm tracks. *J. Climate,* **8,** 1938–1950.

Kiladis, G. N., and K. C. Mo, 1998: Interannual and intraseasonal variability in the Southern Hemisphere. *Meteorology of the Southern Hemisphere,* D. J. Karoly and D. G. Vincent, Eds., Amer. Meteor. Soc., 307–336.

Marques, R. F. C., and V. B. Rao, 1999: A diagnostic of a long-lasting blocking event over the southeast Pacific Ocean. *Mon. Wea. Rev.,* **127,** 1761–1776.

——, and ——, 2000: Interannual variations of blocking in the Southern Hemisphere and their energetics. *J. Geophys. Res.,* **105,** 4625–4636.

Miller, A., 1976: The climate of Chile. *Climates of Central and South America,* W. Schwerdtfeger, Ed., Elsevier, 113–145.

Mo, K. C., and G. H. White, 1985: Teleconnections in the Southern Hemisphere. *Mon. Wea. Rev.,* **113,** 22–37.

——, and M. Ghil, 1987: Statistics and dynamics of persistent anomalies. *J. Atmos. Sci.,* **44,** 877–901.

Montecinos, A., 1998: Seasonal rainfall forecast in central Chile (in Spanish). M.S. thesis, Department of Geophysics, University of Chile, 116 pp.

——, A. Díaz, and P. Aceituno, 2000a: Seasonal diagnostic and predictability of rainfall in subtropical South America based on tropical Pacific SST. *J. Climate,* **13,** 746–758.

——, R. D. Garreaud, and P. Aceituno, 2000b: Interdecadal rainfall variability in subtropical South America and its relationship with tropical Pacific SST. Preprints, *Sixth Int. Conf. on Southern Hemisphere Meteorology and Oceanography,* Santiago, Chile, Amer. Meteor. Soc., 67–68.

Pittock, A. B., 1980: Patterns of climatic variation in Argentina and Chile. Part I: Precipitation, 1931–1960. *Mon. Wea. Rev.,* **108,** 1347–1361.

Pizarro, J. G., and A. Montecinos, 2000: Cutoff cyclones off the subtropical coast of Chile. Preprints, *Sixth Int. Conf. on Southern Hemisphere Meteorology and Oceanography,* Santiago, Chile, Amer. Meteor. Soc., 278–279.

Quinn, W., and V. Neal, 1983: Long-term variations in the Southern Oscillation, El Niño and the Chilean subtropical rainfall. *Fish. Bull.,* **81,** 363–374.

Rao, V. B., S. H. Franchito, and J. P. Reyes-Fernandez, 2000: Comments on ''Blocking over the South Pacific and Rossby wave propagation.'' *Mon. Wea. Rev.,* **128,** 4160–4161.

Renwick, J. A., and M. J. Revell, 1999: Blocking over the South Pacific and Rossby wave propagation. *Mon. Wea. Rev.,* **127,** 2233–2247.

——, and ——, 2000: Reply. *Mon. Wea. Rev.,* **128,** 4162.

Reynolds, R. W., and T. M. Smith, 1994: Improved global sea surface temperature analysis using optimum interpolation. *J. Climate,* **7,** 929–948.

Rubin, M. J., 1955: An analysis of pressure anomalies in the Southern Hemisphere. *Notos,* **4,** 11–16.

Rutllant, J., and H. Fuenzalida, 1991: Synoptic aspects of the central Chile rainfall variability associated with the Southern Oscillation. *Int. J. Climatol.,* **11,** 63–76.

Shukla, J., and K. C. Mo, 1983: Seasonal and geographical variation of blocking. *Mon. Wea. Rev.,* **111,** 388–402.

Sinclair, M. R., 1996: A climatology of anticyclones and blocking for the Southern Hemisphere. *Mon. Wea. Rev.,* **124,** 245–263.

——, J. A. Renwick, and J. W. Kidson, 1997: Low-frequency variability of Southern Hemisphere sea level pressure and weather system activity. *Mon. Wea. Rev.,* **125,** 2531–2543.

Smith, T. M., R. W. Reynolds, R. E. Livezey, and D. C. Stokes, 1996: Reconstruction of historical sea surface temperatures using empirical orthogonal function. *J. Climate,* **9,** 1403–1420.

Trenberth, K. E., 1982: Seasonality in Southern Hemisphere eddy statistics at 500 mb. *J. Atmos. Sci.,* **39,** 2507–2520.

——, 1991: Storm tracks in the Southern Hemisphere. *J. Atmos. Sci.,* **48,** 2159–2178.

——, and K. C. Mo, 1985: Blocking in the Southern Hemisphere. *Mon. Wea. Rev.,* **113,** 3–21.

——, and D. J. Shea, 1987: On the evolution of the Southern Oscillation. *Mon. Wea. Rev.,* **115,** 3078–3096.

Walker, G. T., and E. W. Bliss, 1932: World weather. V. *Mem. Roy. Meteor. Soc.,* **4,** 53–84.

White, W. B., 2000: Influence of the Antarctic Circumpolar Wave on Australian precipitation from 1958 to 1997. *J. Climate,* **13,** 2125–2141.

——, and R. G. Peterson, 1996: An Antarctic Circumpolar Wave in surface pressure, wind, temperature and sea-ice extent. *Nature,* **380,** 699–702.

——, and N. J. Cherry, 1999: Influence of the Antarctic Circumpolar Wave upon New Zealand temperature and precipitation during autumn–winter. *J. Climate,* **12,** 960–976.